



A Biogeochemical Alkalinity Sink in a Shallow, Semi-arid Estuary of the Northwestern Gulf of Mexico

Larissa M. Dias¹ · Xinping Hu¹ · Hang Yin¹

Received: 26 May 2022 / Accepted: 8 December 2022 / Published online: 22 December 2022
© The Author(s) 2022

Abstract

Estuarine total alkalinity (TA), which buffers against acidification, is temporally and spatially variable and regulated by complex, interacting hydrologic and biogeochemical processes. During periods of net evaporation (drought), the Mission-Aransas Estuary (MAE) of the northwestern Gulf of Mexico experienced TA losses beyond what can be attributed to calcification. The contribution of sedimentary oxidation of reduced sulfur to the TA loss was examined in this study. Water column samples were collected from five stations within MAE and analyzed for salinity, TA, and calcium ion concentrations. Sediment samples from four of these monitoring stations and one additional station within MAE were collected and incubated between 2018 and 2021. TA, calcium, magnesium, and sulfate ion concentrations were analyzed for these incubations. Production of sulfate along with TA consumption (or production) beyond what can be attributed to calcification (or carbonate dissolution) was observed. These results suggest that oxidation of reduced sulfur consumed TA in MAE during droughts. We estimate that the upper limit of TA consumption due to reduced sulfur oxidation can be as much as 4.60×10^8 mol day⁻¹ in MAE. This biogeochemical TA sink may be present in other similar subtropical, freshwater-starved estuaries around the world.

Keywords Reduce sulfur oxidation · Estuaries · Biogeochemistry · Alkalinity · Acidification · Northwestern Gulf of Mexico

1 Introduction

Alkalinity, also known as acid neutralizing capacity, is a key component of the carbonate system in seawater (Feely et al. 2010; Wolf-Gladrow et al. 2007). Total alkalinity (TA) typically behaves in a semi-conservative manner (Millero et al. 1993; Wong 1979) whereby TA is a linear function of salinity in most river–ocean mixing scenarios, although it may be locally influenced by biogeochemical reactions (Krumins et al. 2013; Wolf-Gladrow et al. 2007). In many estuaries, TA is subject to hydroclimatic extremes (Liu et al. 2017;

✉ Xinping Hu
Xinping.hu@tamucc.edu

¹ Harte Research Institute for Gulf of Mexico Studies, Texas A&M University-Corpus Christi, 6300 Ocean Dr., Corpus Christi, TX 78412, USA

Table 1 Partial list of sedimentary carbonate dissolution and iron sulfide oxidation reactions and corresponding molar ratios of changes in TA, SO_4^{2-} , Ca^{2+} , and Mg^{2+}

Reaction	$\Delta\text{TA}:\Delta[\text{Ca}^{2+}]$	$\Delta\text{TA}:\Delta[\text{SO}_4^{2-}]$	$\Delta\text{TA}:\Delta([\text{Ca}^{2+}] + [\text{Mg}^{2+}])$
<i>Carbonate dissolution</i>			
(R1) $\text{CaCO}_3 \rightarrow \text{Ca}^{2+} + \text{CO}_3^{2-}$	+2	-	+2
(R2) $\text{Ca}_{0.85}\text{Mg}_{0.15}\text{CO}_3 \rightarrow 0.85\text{Ca}^{2+} + 0.15\text{Mg}^{2+} + \text{CO}_3^{2-}$	+2.35	-	+2
<i>Iron sulfide oxidation reactions^b</i>			
(R3) $\text{FeS}_2 + 3.75\text{O}_2 + 3.5\text{H}_2\text{O} \rightarrow \text{Fe}(\text{OH})_3 + 2\text{SO}_4^{2-} + 4\text{H}^+$	-	-2	-
(R4) $\text{FeS} + 2.25\text{O}_2 + 2.5\text{H}_2\text{O} \rightarrow \text{Fe}(\text{OH})_3 + \text{SO}_4^{2-} + 2\text{H}^+$	-	-2	-

^a Calcite and aragonite^b Only reactions in which O_2 is the oxidant are listed

Murgulet et al. 2018), and complex, interacting hydrologic and biogeochemical processes (Cai et al. 2003; Guo et al. 2008; Langdon et al. 2000; Liu et al. 2017; Murgulet et al. 2018). Low TA levels often render estuaries vulnerable to acidification (Joesoef et al. 2017). Estuarine acidification may negatively affect biological organisms from the species to ecosystem-level (Amara et al. 2012; Dove and Sammut 2007; Marshall et al. 2008). Therefore, studies that investigate TA dynamics are important for understanding estuarine acidification.

Calcium carbonate formation and dissolution are common biogeochemical processes that can affect estuarine TA (Wolf-Gladrow et al. 2007). Carbonate dissolution increases TA, whereas calcification decreases TA (Table 1). The reaction stoichiometry suggests that changes in TA and calcium concentration (for calcium carbonate) or calcium and magnesium concentration combined (for magnesian calcite; Table 1; Berner et al. 1970) follow a 2:1 ratio. In addition to calcification and carbonate dissolution, other biogeochemical processes can also alter TA (Middelburg et al. 2020; Wolf-Gladrow et al. 2007). Some redox reactions (e.g., photosynthesis, denitrification, manganese reduction, iron reduction, and sulfate reduction) increase TA, while other reactions (e.g., aerobic respiration and oxidation of ammonia, hydrogen sulfide, and ferrous iron) decrease TA (Burdige 2007; Emerson and Hedges 2008; Krumins et al. 2013). Atmospheric deposition of acids from natural or anthropogenic sources (primarily sulfur oxides, SO_x and nitrogen oxides, NO_x) can result in TA consumption in coastal areas (Doney et al. 2007; Hunter et al. 2011). Reverse weathering, the opposite chemical reaction of weathering, may also reduce TA in shallow waters (Garrels 1965; Mackenzie and Garrels 1966; Sillen 1961) although its rates are considered slow in the modern oceanic environment (Isson and Planavsky 2018; Michalopoulos and Aller 2004).

Due to the prevalence of seawater sulfate (~28 mM at salinity 35) and relatively high organic carbon content in coastal and estuarine environments, redox cycling of sulfur is an important link in sedimentary metabolism (Canfield and Farquhar 2009). Meanwhile, redox sulfur cycling also has significant implications toward coastal and estuarine TA balance (Table 1; Krumins et al. 2013). In natural marine and estuarine systems, sulfur cycling and carbonate dissolution or precipitation are coupled (Krumins et al. 2013; Luff and Wallmann 2003; Risgaard-Petersen et al. 2012; Yin et al. 2022). However, the reaction stoichiometry may not strictly follow simple reactions as shown in Table 1 (Krumins et al. 2013). For example, when carbonate dissolution ($\Delta\text{TA}:\Delta[\text{Ca}^{2+}]=2:1$) happens along with oxidation of iron monosulfide ($\Delta\text{TA}:\Delta[\text{SO}_4^{2-}]=-2:1$), changes in TA and $[\text{Ca}^{2+}]$, i.e., $\Delta\text{TA}:\Delta[\text{Ca}^{2+}]$ will be less than 2:1. Conversely, calcification and iron sulfide oxidation would result in a $\Delta\text{TA}:\Delta[\text{Ca}^{2+}]$ ratio greater than 2:1 (Table 1).

Although 90% of sedimentary sulfide is reoxidized completely to SO_4^{2-} in marine sediments while the rest is buried (Thamdrup et al. 1994), the oxidation process is complex and involves multiple steps of reactions which are sometimes facilitated by microbes (Jørgensen and Nelson 2004). Iron sulfides are the dominant forms of reduced sulfur in most marine sediments (Risgaard-Petersen et al. 2012), although many other intermediate oxidation products such as elemental sulfur, sulfite, thiosulfate, or polythionates may be present (Burdige 1993; Jørgensen et al. 1990; Jørgensen and Nelson 2004; Thamdrup et al. 1994; van den Ende and Gernerden 1993). Complete and partial oxidation of iron sulfides is common in sediments, and these compounds are also commonly oxidized by manganese oxides, NO_3^- , $\text{Fe}(\text{OH})_3$, and other compounds (Aller and Rude 1988; Canfield et al. 1993; Jørgensen and Nelson 2004; Luther et al. 1982; Schippers and Jørgensen 2001, 2002).

The Mission-Aransas Estuary (MAE) is a semiarid, long-residence time (360 d; Solis and Powell 1999), and nitrogen limited (Mooney and McClelland 2012) estuary in the

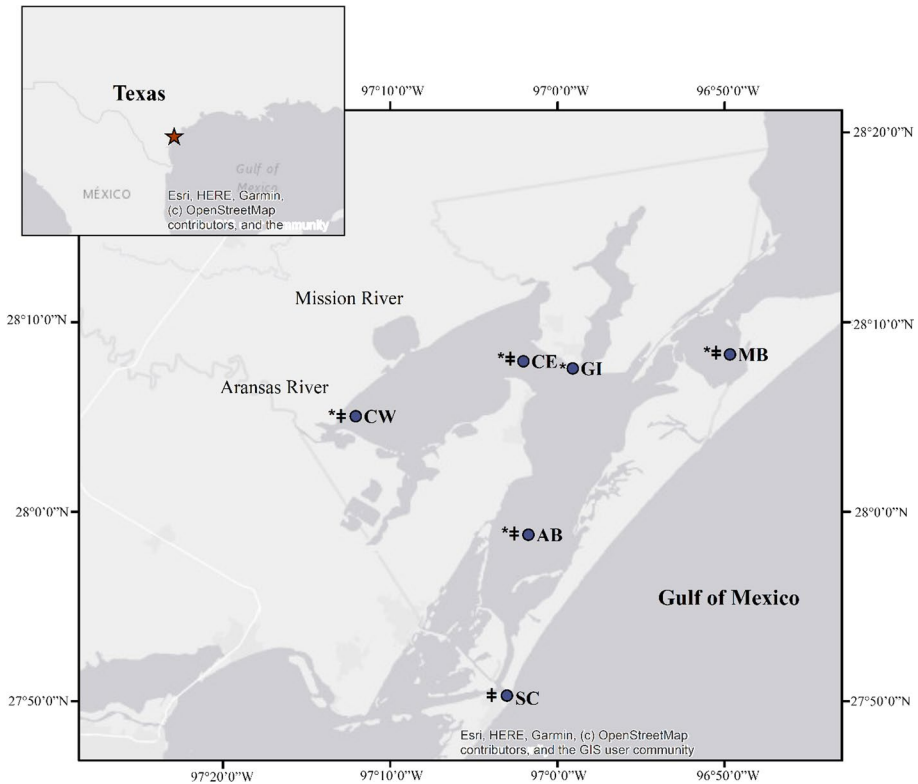


Fig. 1 Sampling sites (closed circles), categorized as sediment core collection sites (*) and the reserve's System Wide Monitoring Program monitoring stations (#) within Mission-Aransas Estuary. Inset map shows the location (star) relative to the Gulf of Mexico

northwestern Gulf of Mexico (nwGOM). This estuary has experienced multidecadal declines in both TA and pH (Hu et al. 2015). It is known that MAE is the southernmost commercial oyster fishing ground in this region (Pollack et al. 2013), and freshwater inflow reduction may be a reason for declining TA (Hu et al., 2015). Meanwhile, the presence of pyrite (Buzas-Stephens et al. 2018) also indicates that observed TA loss could be attributed to sediment redox processes beyond biogenic carbonate precipitation (e.g., oyster shell formation). This study hence explored the possible sulfide oxidation mechanism that contributes to the observed TA loss. Changes in TA and ionic concentrations (calcium, magnesium, and sulfate) of the estuarine water column, overlying water of incubated sediment, and sediment slurries from MAE, were examined, and the reaction stoichiometry in this system was determined.

2 Methods

2.1 Study Area

MAE is a National Estuarine Research Reserve (NERR) and contains abundant oysters (*Crassostrea virginica*) and blue crabs (*Callinectes sapidus*), both economically and ecologically important species, and provides wintering habitat for the only sustained wild population of endangered whooping crane (*Grus americana*; Pollack et al. 2013; Weatherall et al. 2018). MAE is a well-mixed, shallow (average depth 2 m), bar-built estuary of 540 km² bordering the nwGOM (Pollack et al. 2013). It consists of a primary bay, Aransas Bay, that is connected to the nwGOM through the Aransas Ship Channel, and two secondary bays, Copano and Mesquite Bays, that receive freshwater input (Fig. 1; Pollack et al. 2013). The main sources of freshwater inflow to Copano Bay are the Mission and Aransas Rivers (Mooney and McClelland 2012), and Mesquite Bay receives freshwater from San Antonio Bay during flood periods. Evaporation is approximately two times of precipitation on average. MAE hosts one of the largest relative differences between average maximum and minimum monthly inflows in the GOM (Solis and Powell 1999). Sediments consisting of Pleistocene sand, silt, and mud originate from the Rio Grande Prairie and enter the estuary through the Mission and Aransas Rivers (TDWR 1982). This oligotrophic estuary is subject to long periods of low freshwater inflow interspersed with short but high-magnitude flooding periods (Mooney and McClelland 2012; TDWR 1982; Yao and Hu 2017), creating a unique study environment from a biogeochemical standpoint.

2.2 Field sampling

From 2014 to 2021, monthly or fortnightly surface and bottom water samples were collected using a Van Dorn water sampler from the five long-term System Wide Monitoring Program (SWMP) stations: Copano West (CW), Copano East (CE), Aransas Bay (AB), Mesquite Bay (MB), and Aransas Ship Channel (SC) (Fig. 1), established by the Mission-Aransas NERR as a part of a nationally coordinated program that tracks a variety of biological, physical, and chemical parameters (Evans et al. 2012; Yao and Hu 2017). Sample

Table 2 Sampling location, collection date, and identification number of sediment cores and slurry sample collected in Mission-Aransas Estuary

Sampling location	ID	Latitude	Longitude	Collection date
Copano Bay West (CW)	1	−97.201	28.084	02/22/2018
Aransas Bay, Goose Island (GI)	2	−96.984	28.126	05/31/2018
Aransas Bay, Goose Island (GI)	3	−96.984	28.126	05/31/2018
Aransas Bay (AB)	4	−97.029	27.980	09/19/2018
Aransas Bay (AB)	5	−97.029	27.980	03/27/2019
Copano Bay West (CW)	6	−97.201	28.084	03/27/2019
Mesquite Bay (MB)	7	−96.828	28.138	03/27/2019
Copano Bay East (CE)	8	−97.034	28.132	02/09/2021
Copano Bay East (CE)	9	−97.034	28.132	02/09/2021
Copano Bay West (CW)	Slurries	−97.201	28.084	10/05/2021

collection followed the standard protocol for ocean CO₂ studies (Dickson et al. 2007). Water for TA analysis was collected in 250 mL borosilicate glass bottles and preserved with 100 µL saturated HgCl₂ solution (Dickson et al. 2007). For surface water only, Ca²⁺ samples were collected in 125 mL polypropylene bottles. All samples were refrigerated at 4 °C until analyses (Yao and Hu 2017). The water column was mostly well mixed throughout the sampling period except during high freshwater inflow events (Hu et al. 2022).

Between February 2018 and October 2021, nine sediment cores (~15 cm, 1–9) followed by two sediment slurry samples (upper ~15 cm, A and B) and one control seawater sample (C) were collected from four of the five NERR stations (Fig. 1; Table 2). One additional station located in Aransas Bay and adjacent to Goose Island State Park (GI) was also sampled for sediment cores. Station locations were chosen based on data availability and to represent a variety of estuarine hydrologic conditions (Yao and Hu 2017). Immediately after collection, rubber stoppers were replaced and sealed with electrical tape before being transported to the lab. Slurry samples were also collected with core samplers using the same methods and were later processed in the lab.

The Texas Commission on Environmental Quality (TCEQ) reported that average sulfur dioxide (SO₂) in Corpus Christi averaged 0.3 ± 0.2 ppb and nitrogen oxides (NO_x) near the City of Corpus Christi (Karnes City, ~150 km away) averaged 4.8 ± 5.0 ppb in October of 2022 (TCEQ 2022; https://www.tceq.texas.gov/cgi-bin/compliance/monops/monthly_summary.pl?cams=1070), and little influence in the more remote vicinity of MAE was expected. However, to ensure that the nearby Intracoastal Waterway was not causing significant atmospheric acid deposition, Ogawa ambient air passive samplers for NO₂ and SO_x were placed at the CE station in spring of 2021. Samplers consisted of a double-sided (two per sampler) end cap and stainless-steel screen (allowing for passive diffusion) equipped with an internal pre-coated pad obtained from Ogawa (Felix and Elliott 2014; Ogawa & Co., USA 2006). Pads were changed every 17–43 days during water sampling trips, and travel “blank” pads for NO₂ and SO_x were carried on each sampling trip to account for pollution arising from the boat and vehicle during transportation.

2.3 Laboratory Analyses

2.3.1 Sediment Core Incubations: Phase I

Phase I of the incubation study aimed to document and analyze reaction stoichiometry between TA, [Ca²⁺], and [SO₄²⁻] in MAE. Sediments were collected in MAE for cores 1–7 with intact overlying surface water (Table 2) and were incubated for extended periods (6–8 weeks, depending on availability of surface water in cores). Surface water was added to cores which experienced depleted initial surface water, after which cores were treated as new specimens. The cores were opened within 7 days of collection, and water was stirred daily to maintain aeration. The shallow nature of cores and stirring was designed to ensure overlying water oxygenated. Surface water salinity was measured twice per week with a Thermo Scientific ORION Star A212 benchtop salinometer (Yao and Hu 2017) and maintained within ±0.1 the original value by adding Milli-Q water.

During each sample collection, two duplicate 25 mL screwcap glass scintillation vials for TA titration were filled with 20 mL surface water and treated with 25 µL saturated HgCl₂ solution. Two weekly 2 mL surface water samples were also collected in snap cap vials for Ca²⁺ analyses. For cores 4–7, two weekly 2 mL surface water samples for SO₄²⁻ analyses were collected and filtered through a 0.45 µm filter. All samples were stored in

a 4 °C refrigerator until analyses, which occurred within 3 months of sample collection. After > 7 weeks of incubation, results were inconsistent due to depletion of sedimentary organic matter, and were not included in figures, although supplementary tables include all data.

2.3.2 Sediment Core Incubations: Phase II

Phase II of the incubation study aimed to quantify changes in ion ratios and TA caused by sediment reactions under increasing salinity conditions. Sediments from cores 8 and 9 (Table 2) were incubated for 3 weeks without overlying water salinity adjustment to simulate evaporation-dominated conditions during drought period. Core 8 was exposed to air immediately upon collection, whereas core 9 was maintained in anoxic conditions for 4 weeks prior to opening. The overlying water was continuously stirred to maintain aeration. Surface water salinity was measured weekly using the same approach above. Water samples were collected at the beginning and the end of the 3-week incubation period. Samples for TA were collected following the same methods in Phase I. Two duplicate 5 mL surface water samples were collected for Ca^{2+} and Mg^{2+} analyses, and two duplicate 2 mL surface water samples for sulfate analyses were also collected and filtered through a 0.45 μm filter. All samples were stored at 4 °C until analyses within 3 months.

2.3.3 Slurry Incubations

The effect of sediment redox reactions on water TA was examined by incubating sediment slurries with continuous exposure to air. Within 24 h of bulk sediment collection from CW, sediments were firstly filtered through a 0.5 mm pore size sieve and fine sediments were collected. Slurries were set up by mixing ~ 100 mL sediment (150 and 151 g for slurry A and B, respectively) with 1000 mL water collected from CE. A control with 1200 mL water from CE station was also set up. The slurries were incubated in an open container in the dark (to prevent photosynthesis) with continuous stirring. Salinity was measured during the incubation. After the incubation, the slurries were then centrifuged at 3000 rpm for 10 min, and supernatant water was filtered through a 0.2 μm filter. Filtered and centrifuged water was collected for TA following the procedures for core incubations (see Sects. 2.3.1 and 2.3.2). Samples for ions analyses (Mg^{2+} , Ca^{2+} , and SO_4^{2-}) were collected in 5 mL glass scintillation vials. pH was monitored using an Orion™ Ross™ glass electrode (calibrated daily; NBS scale) every 1–4 h during the day on days 1–3, and then twice daily on days 4–7 and 10. Salinity was measured once daily at the time of sample collection. Samples were collected on days 1, 2, 3, 5, 7, and 10.

2.3.4 Chemical Analyses

TA for incubations, slurries, and water samples was titrated with a 0.1 M HCl (in 0.5 M NaCl) using an AS-ALK2 alkalinity titrator (Apollo SciTech) with a precision of $\pm 0.1\%$. Temperature of the titration vessel was maintained at 22 ± 0.1 °C with a water bath, and certified research materials (Dickson et al. 2003) was used to ensure the titration accuracy. For Phase I sediment cores and water samples, potentiometric titration for Ca^{2+} was conducted (Kanamori and Ikegami 1980) using EGTA as the titrant and a Calcium ion-selective electrode

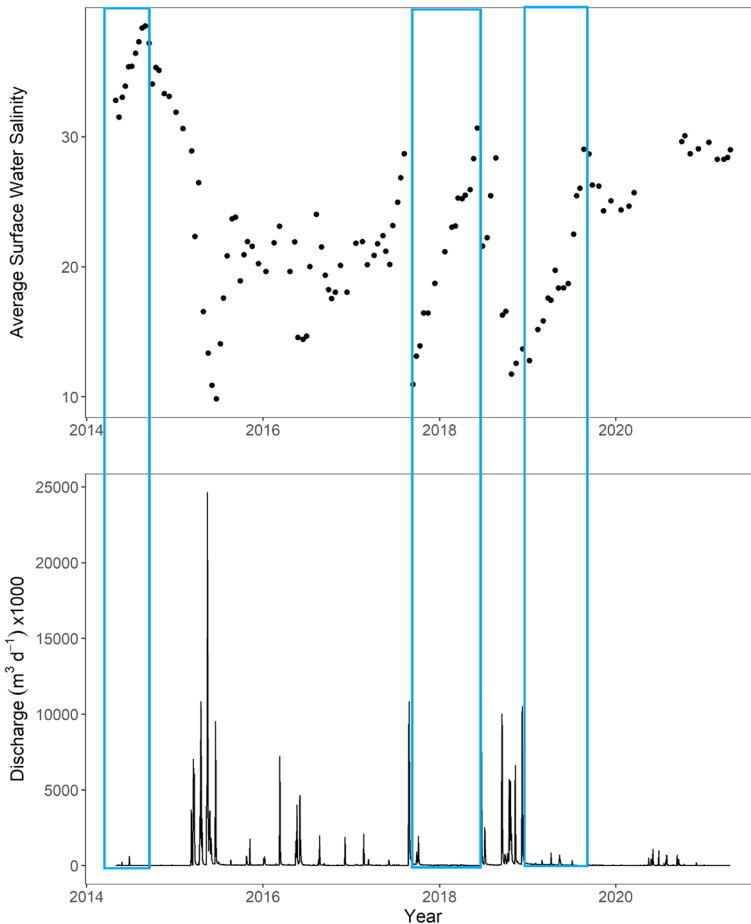


Fig. 2 Evaluation of “lagoonal” or evaporative periods in Mission-Aransas Estuary (blue rectangles), distinguished by low freshwater inflow and increasing salinity. Freshwater discharge is sum from Mission and Aransas Rivers at USGS stations 08189500 and 08189700, respectively

(Metrohm) to detect the endpoint, with a precision of $\pm 0.2\%$. A Dionex High Performance Ion Chromatograph (Model DX600, Dionex Corp., Sunnyvale, California) was used to determine SO_4^{2-} concentrations (Murgulet et al. 2018). The lower detection limit of the method was ~ 1.0 mM, depending on the background signal of measured constituents in the samples, with a precision of ± 0.1 mM (1σ ; Murgulet et al. 2018).

Samples for Mg^{2+} , Ca^{2+} , and SO_4^{2-} from Phase II core incubations and slurries were diluted approximately 50-fold with ultrapure 1% HNO_3 containing 2 ppb In as an internal standard. Samples were analyzed using a sector-field ICP-MS (ThermoFisher Element XR) with a PC3 Peltier spray chamber (Elemental Scientific) for sample introduction. All elements were analyzed in medium resolution. Calibration was performed using external standards which were checked by comparison with an aliquot of standard seawater, with a precision of 2–2.5% (A. Schiller, *personal communication*).

Pads from all passive air samplers (NO_2 and SO_x) were eluted with 5 mL of Milli-Q water within 24 h of retrieval, and NO_2 and SO_x concentrations were analyzed within 14 days of pad retrieval. NO_2 pads were analyzed following protocol from Felix and Elliott (2014) with a Thermo Evolution 60S UV–vis. SO_x pads were analyzed with a Dionex Ion Chromatograph 4000i using 1.8 mM Na_2CO_3 +1.7 mM NaHCO_3 as eluant, with 1.7 mL min^{-1} flow rate and 100 μL sample loop (Ogawa & Co., USA 2006) with a detection limit of 0.02 mg L^{-1} and precision of $\pm 0.3\%$. Ogawa sampler protocol was used to calculate NO_2 air concentrations by correcting for temperature and relative humidity (Ogawa & Co., USA 2006), with a precision of $\pm 0.2\%$.

2.4 Water Column Stoichiometric Calculations

Freshwater discharge information for Mission and Aransas Rivers was obtained from US Geological Survey (USGS) streamgages 08189500 and 08189700, respectively (USGS 2021). Visual inspection of data revealed periods of time whereby the estuary was in a “lagoonal” state, or an evaporation-dominated condition, by declining freshwater discharge accompanied by increasing salinity (Fig. 2). Three prolonged evaporation-dominated periods were identified from visual inspection prior to and during the timeframe of sediment incubation experiments, 1. 05/02/2014 to 12/9/2014 (also see Fig. 3), 2. 01/01/2018 to 06/18/2018, and 3. 02/13/2019 to 09/12/2019. Time series changes in salinity-corrected $[\text{Ca}^{2+}]$ and TA in each of the “lagoonal” periods were calculated to identify consumption or production (Fig. 4). To calculate concentration changes (Δ) for water column samples (ΔTA and $\Delta[\text{Ca}^{2+}]$), we compared linear regression coefficient of these salinity-corrected values between two consecutive samplings (Eq. 1), and those obtained between each time point and the initial values (Eq. 2) for the three evaporative periods, using Eqs. (1, 2),

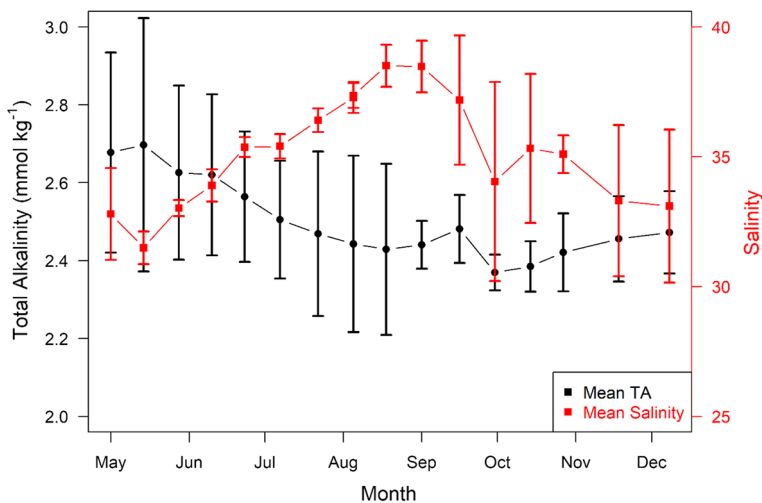


Fig. 3 Time series of mean TA and salinity from surface water data collected at Mission-Aransas Estuary during the 2014 drought (lagoonal period I, May–December 2014). Error bars represent the standard deviation from the mean for all stations within the estuary ($n=5$)

Table 3 Annual precipitation recorded at the Copano East field station in Mission-Aransas Estuary or for TWDB quadrant 910, which encompasses the CE station (marked with an *) and total freshwater discharges from Mission and Aransas Rivers at USGS streamgage locations

Year	Total precipitation (mm)	Total freshwater discharge (m ³)
2014	583.2	48.3
2015	1062.0	2786.2
2016	880.6	783.7
2017	829.8*	772.6
2018	1042.2*	2814.4
2019	748.7	225.6
2020	699.8	185.0
2021	1221.6	3022.8

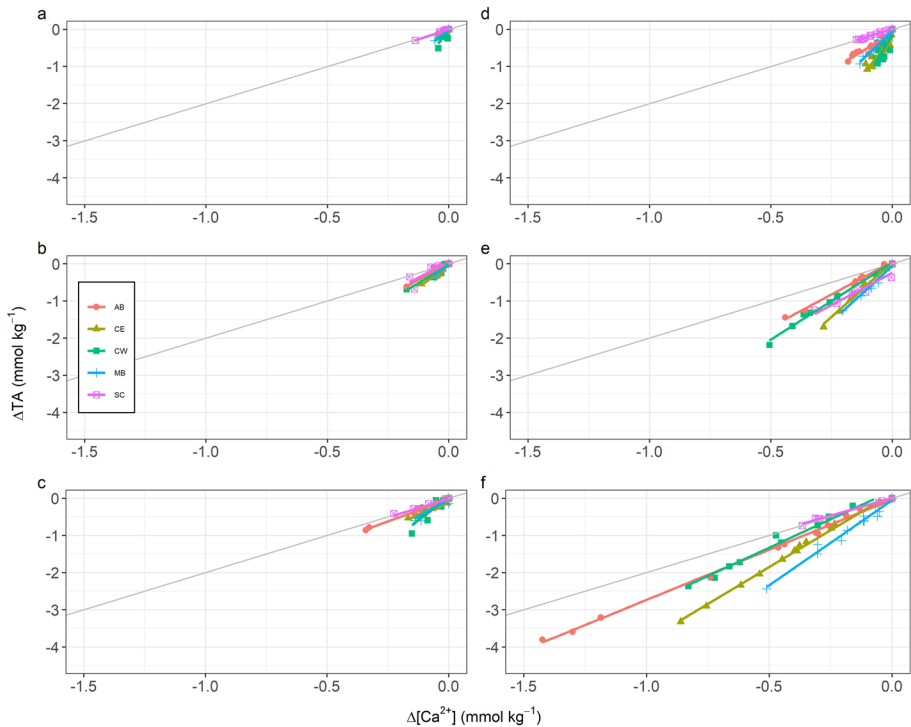


Fig. 4 $\Delta\text{TA}:\Delta[\text{Ca}^{2+}]$ relationships in three evaporation-dominated periods in Mission-Aransas Estuary. $\Delta\text{TA}:\Delta[\text{Ca}^{2+}]$ were calculated using both Eq. (1) (a–c) and Eq. (2) (d–f). **a** and **d** represent evaporation-dominated period I from 5/2/14 to 12/9/14. **b** and **e** represent evaporation-dominated period II from 1/1/18 to 6/18/18. **c** and **f** represent evaporation-dominated period II from 2/13/19 to 9/12/19. The solid gray line represents the relationship of $\Delta\text{TA}:\Delta[\text{Ca}^{2+}]$ from calcification, with a theoretical slope of 2 (i.e., CaCO_3)

$$\Delta = X_{(i+1)} - \frac{X_i}{S_i} \times S_{(i+1)} \quad (1)$$

$$\Delta = X_i - \frac{X_0}{S_0} \times S_i \tag{2}$$

where X_i is the i th and X_0 is the initial measurement for each variable (TA or $[\text{Ca}^{2+}]$) and S_i is the i th and S_0 is the initial measurement for salinity. Different calculation methods were used because mixing of water masses during time series water column sampling might interfere with ion and TA concentrations and hence comparison with prior measurements (Eq. 1) would be a more accurate measure of change than comparison with initial measurements across several months (Eq. 2). When salinity varied in an incubation and the slurry experiments, all samples were referenced to the initial values (Eq. 2). Propagated uncertainties for ΔTA , $\Delta[\text{Ca}^{2+}]$, $\Delta[\text{Mg}^{2+}]$, and $\Delta[\text{SO}_4^{2-}]$ ranged from 0.00–0.02, 0.02–0.45, 0.18–2.06, and 0.14–1.06 mmol kg^{-1} , respectively.

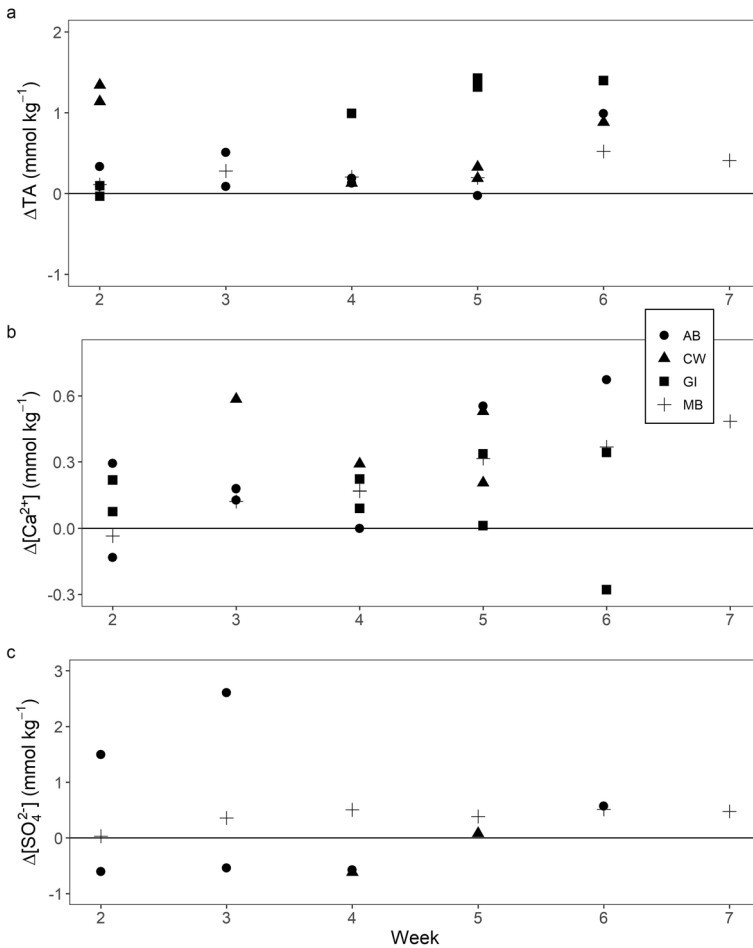


Fig. 5 Time series of **a** ΔTA , **b** $\Delta[\text{Ca}^{2+}]$, and **c** $\Delta[\text{SO}_4^{2-}]$, grouped by collection location of phase I cores (one through seven) and calculated compared to original measurements using Eq. (2). Week is number of weeks after collection

2.5 Auxiliary Data

Precipitation data for 2014–2016 and 2019–2021 were obtained from the NERR Centralized Data Management Office's Data Graphing and Export System (<http://cdmo.baruch.sc.edu/dges/>). Precipitation data for 2017 and 2018 were obtained from the Texas Water Development Board's (TWDB 2021) Water Data for Texas portal (<https://waterdatafortexas.org>; TWDB 2021). Discharge data (parameter code 00060) were obtained for the Mission (UID# 08189500) and Aransas (UID# 08189700) Rivers (USGS 2021) and were downloaded with the function “importDVs” available in the R package “water-Data” (Ryberg and Vecchia 2012).

3 Results

3.1 Surface Water

MAE experienced a loss of TA accompanied by increasing salinity between May and September of 2014 (Fig. 3), a drought year with low precipitation and freshwater inflow from the Mission and Aransas Rivers (Fig. 2; Table 3). Analyses of surface water samples collected in MAE in 2014 suggested that TA loss was accompanied by a loss of $[\text{Ca}^{2+}]$, and the calculated $\Delta\text{TA}:\Delta[\text{Ca}^{2+}]$ ratio was greater than 2:1 during the evaporative period using both calculation methods (Fig. 4a, d).

Similar to 2014, during another two drought periods, water samples collected from MAE between January 2018 and December 2021 also had $\Delta\text{TA}:\Delta[\text{Ca}^{2+}]$ ratios greater than 2:1 (Fig. 4b, c, e, f). The ratios were not as high as those observed during 2014, and higher ratios were found at MB, CW, and CE stations, while AB and SC stations were similar and had TA consumption rates slightly greater than predicted from calcification alone.

3.2 NO_2 and SO_x

There was an average 1.67 ppb NO_2 in atmospheric measurements collected at CE in spring 2021. Only one of the SO_x pads had detectable values (0.0002 ppb) and the rest were below the detection limit. This level of NO_2 and SO_x is lower than average worldwide concentration (WHO 2010), and below OSHA and European Union International standards for hazardous substances (Bozkurt et al. 2018; European Commission 2000; NIH 2022).

3.3 Sediment Incubations

3.3.1 Phase I Core Incubations

In Phase I core incubations when salinity was maintained constant, overlying water TA, Ca^{2+} , and SO_4^{2-} concentrations generally increased with time, indicating net productions of TA, Ca^{2+} , and SO_4^{2-} (Fig. 5, Table S1) with some exceptions. For example, TA decreased $0.68 \text{ mmol kg}^{-1}$ in a CW core following 3 weeks of incubation (Fig. 5a), $[\text{Ca}^{2+}]$ decreased $0.28 \text{ mmol kg}^{-1}$ in a GI core following 4 weeks of incubation (Fig. 5b), and

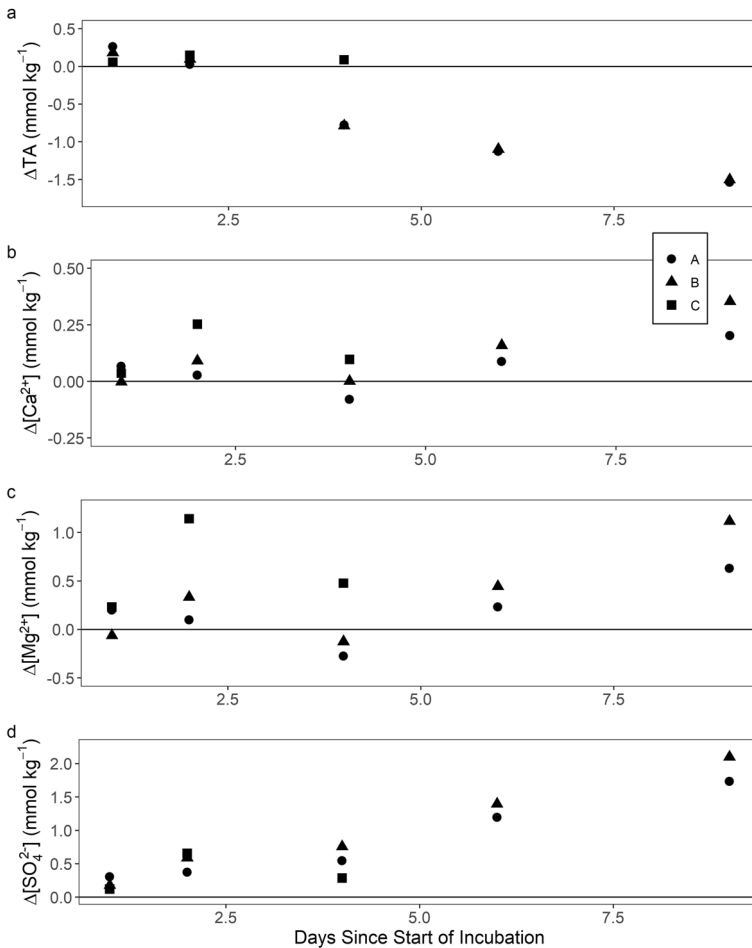


Fig. 6 Change in **a** TA, **b** $[\text{Ca}^{2+}]$, and **c** $[\text{Mg}^{2+}]$, and **d** $[\text{SO}_4^{2-}]$ concentrations since the original measurements (t_0) for slurries calculated using Eq. (2)

$[\text{SO}_4^{2-}]$ decreased $1.00 \text{ mmol kg}^{-1}$ in an AB core following 4 weeks of incubation (Fig. 5c; Table S.1).

3.3.2 Phase II Core Incubations

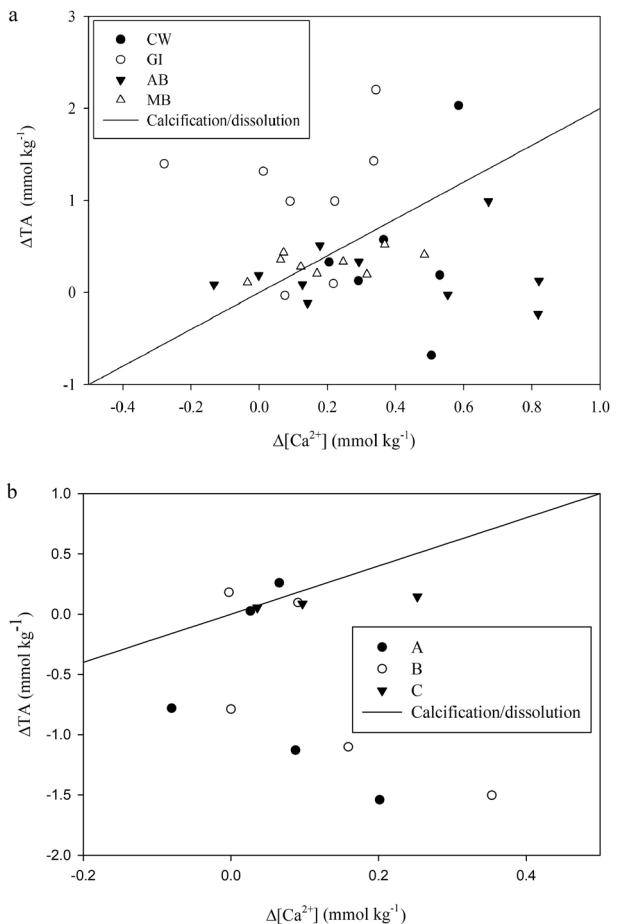
In Phase II core incubations, salinity was not maintained to simulate evaporation under drought conditions. As a result, overlying water salinity increased from 27.7 to 50.5 within 2 weeks in core 8 and 27.7–38.8 with 3 weeks in core 9, both from CE (Table S2). After accounting for the evaporation effect, core 8 had a TA decrease of $0.51 \text{ mmol kg}^{-1}$, $[\text{Ca}^{2+}]$ increase of $2.52 \text{ mmol kg}^{-1}$, $[\text{SO}_4^{2-}]$ increase of $2.46 \text{ mmol kg}^{-1}$, and $[\text{Mg}^{2+}]$ decrease of -1.28 mM (Table S2). Even though core 9 did not have as large of a salinity increase during a longer incubation, TA decreased by $2.60 \text{ mmol kg}^{-1}$, $[\text{Ca}^{2+}]$ increased by $0.10 \text{ mmol kg}^{-1}$, and $[\text{SO}_4^{2-}]$ increased by $2.09 \text{ mmol kg}^{-1}$ (Table S2). It should be noted that core 9 was maintained under anoxic conditions for 4 weeks prior to air exposure and hence could

have produced additional iron sulfide during this time, leading to the faster TA decrease in this incubation from the initial value, which was much higher than core 8. However, for the duplicate $[Mg^{2+}]$ analysis the results were very different, likely due to sample handling artifact, hence the result was not considered here.

3.3.3 Slurries Incubation

Both the slurry incubations (A and B) and the control (C) showed slight salinity increases during the 10-day incubations, i.e., from ~9 to 10–11 (Table S3). The control had no sediment present, and salinity-corrected TA changed very little ($<0.15 \text{ mmol kg}^{-1}$). In comparison, both A and B exhibited significant increases in salinity adjusted $[Ca^{2+}] + [Mg^{2+}]$ (0.83 and $1.47 \text{ mmol kg}^{-1}$, respectively) and $[SO_4^{2-}]$ (1.73 and $2.10 \text{ mmol kg}^{-1}$, respectively) while salinity adjusted TA decreased by $\sim 1.5 \text{ mmol kg}^{-1}$ in both cases (Fig. 6; Table S3). Along with TA decrease, pH values in both A and B showed faster decrease rates than the control (Fig. S1).

Fig. 7 Changes in TA and $[Ca^{2+}]$ for phase I sediment incubation experiments (a) and slurry experiments (b), calculated using Eq. (2). Solid line is the theoretical changes in TA and $[Ca^{2+}]$ from carbonate dissolution or calcification (with a slope 2)



4 Discussion

4.1 Water Column TA Reduction Under Low Freshwater Input Conditions

Due to its semiarid nature, MAE usually received low freshwater input from Aransas and Mission Rivers in the last decade (Fig. 2; Table 3), which was punctuated by large pulses of river input from storm events (Yao and Hu 2017). Under the low freshwater input conditions, estuarine water in the lagoonal state underwent mostly evaporation, and average evaporation between 2014 and 2021 was 0.34 cm day^{-1} , or $7.71 \times 10^4 \text{ m}^3 \text{ h}^{-1}$ (TWDB 2021). Therefore, an evaporation-reaction approach was necessary to explore reaction stoichiometry during the low freshwater inflow period, i.e., the lagoonal state. Both calculation approaches (Eqs. 1 and 2) revealed that TA and Ca^{2+} consumptions occurred in MAE during the lagoonal state (Fig. 4). While these decreases indicated carbonate precipitation (as shown by the salinity adjusted Ca^{2+} decrease), which is supported by the abundant presence of shellfish species in this estuary (Pollack et al. 2013), the reaction ratio between ΔTA and ΔCa^{2+} did not follow the 2:1 relationship. Rather, TA consumption (ΔTA) was always greater than carbonate precipitation alone, suggesting an additional TA sink.

Major factors that contribute to aquatic TA reduction, other than carbonate formation, include acid production processes that involve nitrogen (nitrification) and reduced sulfur oxidation, which is often associated with the oxidation of metals (Wolf-Gladrow et al. 2007). It is known that estuarine nitrate concentration is low (several μM or lower) under low river inflow conditions (Bruesewitz et al. 2013). Therefore, redox reactions

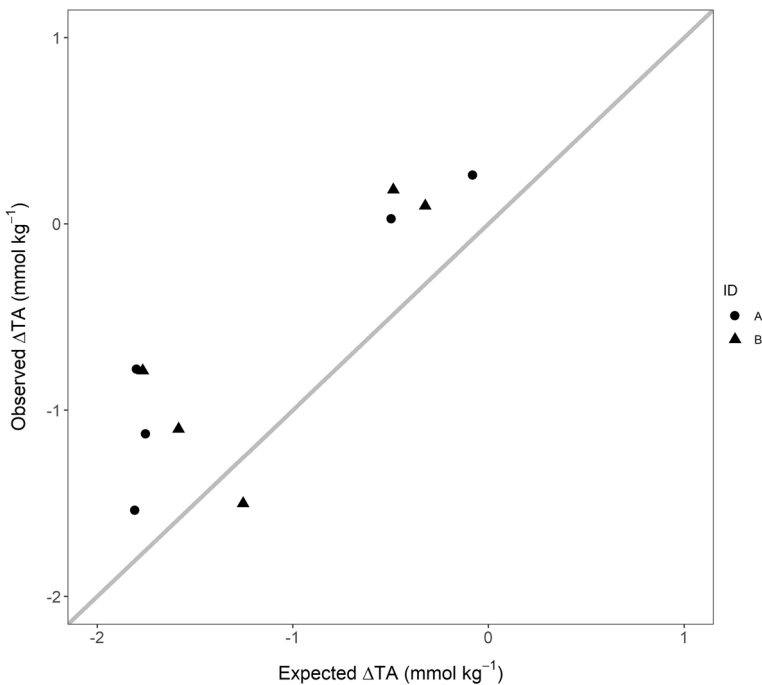


Fig. 8 Expected ΔTA (calculated by ion concentration changes, $2 \times \Delta([\text{Ca}^{2+}] + [\text{Mg}^{2+}]) - 2 \times \Delta[\text{SO}_4^{2-}]$) and observed ΔTA for the slurry incubations

involving nitrogen species were unlikely the cause for the observed TA decrease. The following lab-based incubation experiments provide evidence on the interactions between sulfur cycle and the observed TA consumption.

Sulfate was consistently produced in most incubation experiments (both the whole core and slurry incubations), suggesting oxidation of reduced sulfur species (such as pyrite and iron monosulfide) from estuarine sediments (Jørgensen 1977; Moses et al. 1987). Faster sulfate enrichment was observed in the first month for some of the Phase I cores. However, it should be noted that uncertainty in SO_4^{2-} measurements and propagated uncertainty of ΔSO_4^{2-} values in incubations was non-trivial relative to the measured and calculated values (up to 2.5% of measured value, and 5–100% of the calculated Δ value; see Figs. 5c and 6d, and Tables S1–S3). Nevertheless, even Phase I incubations (with constant salinities), which had the highest variability in results, net production of TA, Ca^{2+} , and SO_4^{2-} was evident (Figs. 5 and 7a and Table S1). In comparison, Phase II and slurry experiments were more consistent in showing the correlations between concentration changes in TA, Ca^{2+} , and SO_4^{2-} (Figs. 6 and 7b; Tables S2 and S3).

In Phase I incubations, other than the GI cores that were collected next to the edge of saltmarshes and those that were re-supplied with overlying water when the original overlying water nearly depleted due to sampling, most data points fell below the 2:1 line between ΔTA and $\Delta[\text{Ca}^{2+}]$ line (i.e., carbonate dissolution or precipitation; Fig. 7a). The GI cores may contain significantly more organic carbon because of their close proximity to the saltmarsh, while all other cores were collected in open water. Organic-rich GI sediments may have stronger continued benthic TA generation derived from anaerobic respiration (Hu and Cai 2011). The slurry incubation also suggested deviation from the simple 2:1 reaction stoichiometry (Fig. 7b). These observations indicated that TA was partially consumed through other sedimentary reactions, likely the production of sulfuric acid as indicated by the increased $[\text{SO}_4^{2-}]$ (Table 1).

In the incubation of core 8 (Phase II), SO_4^{2-} production (2.46 mM) was equivalent to acid production of 4.92 mM (in 21 days). Though $[\text{Ca}^{2+}]$ increase (2.52 mmol kg^{-1}) would suggest TA release of 5.04 mmol kg^{-1} due to CaCO_3 dissolution, the reduction of $[\text{Mg}^{2+}]$ (1.28 mmol kg^{-1}) then would consume 2.56 mmol kg^{-1} TA if Mg-calcite was produced. Theoretically, the ion charge balance would have resulted in a net TA change of $(-4.92 + 5.04 - 2.56) = -2.44$ mmol kg^{-1} . However, the observed ΔTA in this incubation was -0.51 mmol kg^{-1} . This discrepancy suggests that benthic anaerobic process continued to supply TA while the surface preserved reduced sulfur was being oxidized. A caveat is that this discrepancy could be attributed to analytical uncertainty as the propagated errors were non-trivial (Tables S2 and S3). Therefore, to remove the effect of TA flux across the sediment–water interface involved in core incubations, ion and TA changes in the slurry incubations would be a better approach in revealing the reaction stoichiometry. The same approach was taken to calculate the expected TA change due to sulfuric acid production minus that from carbonate dissolution (based on $[\text{Ca}^{2+}]$ and $[\text{Mg}^{2+}]$ changes), and the calculated values agreed reasonably well with the measured ΔTA (Fig. 8; Table S4).

TA consumption due to reduced sulfur oxidation may differ in nature due to abiotic factors such as reaction kinetics. First, Morse (1991) found that < 19% of marine sedimentary pyrite was oxidized within 1 day for anoxic sediments suspended in seawater in equilibrium with the atmosphere, with only 20% of the remaining pyrite oxidation within 7 days and the remaining pyrite having very slow oxidation rates due to coatings such as iron oxide. Given that reaction rates in our incubations would likely be faster than those in nature because of continuous stirring, we would expect faster oxidation of uncoated (lacking a buildup of

iron oxide) pyrite than under natural conditions, making our predictions of sulfide oxidation (hence TA consumption) more rapid. Further investigation is needed to understand the influence of reaction kinetics on TA consumption in situ and whether natural rates align with those observed in incubation experiments. Additionally, the final product of reduced sulfide oxidation might not be sulfate. Other products of sulfide oxidation like sulfite were not quantified in this study. Contributions of organic alkalinity to TA in MAE, especially at low salinity, may be important and should be considered in future studies as well (Abril et al. 2015; Yao and Hu 2017).

Between the different incubation approaches, i.e., varying salinity or consistent salinity and whole core or slurry incubations, TA and cation concentration changes showed different patterns, yet all pointed to a consistent TA reduction at the expense of reduced sulfur oxidation. These independent experiments all suggested that the oxidation of sedimentary reduced sulfur was able to titrate water column TA during stagnant water residence.

4.2 Other Possible Contributors to TA in MAE

Hunter et al. (2011) calculated atmospheric acid concentration changes in the North Sea, Baltic Sea, and South China Sea. For these three regions (North, Baltic, and South China Seas, respectively), addition of SO_x was 0.67, 0.043, and $0.50 \mu\text{M year}^{-1}$ for $f[\text{H}_2\text{SO}_4]$, and NO_x was 1.33, 0.086, and $0.40 \mu\text{M year}^{-1}$ for $f[\text{HNO}_3]$, where $f[X]$ is the annual increase in the concentration of X in the affected water mass as a result of uptake from the atmosphere (Tsyro and Berge 1997). These three regions have SO_2 and NO_2 values that are much higher (15–73 ppb for NO_2 and 3.5–25 ppb for SO_2 ; Chong et al. 2015; Lee et al. 2018; Walden et al. 2021) than what we observed for MAE (1.67 ppb for NO_2 and ≤ 0.002 for SO_2). Since MAE occupies a rural and low-shipping traffic region despite the fact that second largest US port for oil and gas export (Port Corpus Christi) is located nearby, depositions of $0.04\text{--}0.67 \mu\text{M year}^{-1}$ for $f[\text{H}_2\text{SO}_4]$ and $0.09\text{--}1.33 \mu\text{M year}^{-1}$ for $f[\text{HNO}_3]$ were likely the upper limits in the studied region. These values were much smaller than the observed TA decrease. High-sulfur diesel was banned within the US Exclusive Economic Zone (EEZ) in the late 2000s and stricter regulations of sulfur content of shipping fuel have been implemented in recent years (Slaughter et al. 2020). However, future changes in ship traffic and urbanization (Murdock et al. 2014) could lead to increased levels of these gases and greater TA consumption in the estuary, hence continuing atmospheric NO_x and SO_x monitoring is needed.

4.3 The Significance of Benthic TA Consumption

Slurry incubation data was used to estimate the total TA consumption rate (mol d^{-1}) in MAE.

$$\text{Total Alkalinity Consumption} = \frac{\Delta\text{TA} \times v_e}{d_i} \quad (3)$$

where ΔTA is the total change in TA over the entire incubation (mol m^{-3}), v_e is the volume of MAE (m^3), and d_i is the total number of days of incubation. Based on calculated overall TA consumption of 1.52 mol m^{-3} from the 9-day experiment and total volume of $1.08 \times 10^9 \text{ m}^3$ of MAE, we estimated that $1.83 \times 10^8 \text{ mol day}^{-1}$ of TA consumption could

occur due to the combined biogeochemical processes of carbonate dissolution and reduced sulfur oxidation in MAE. In the absence of carbonate dissolution, reduced sulfur oxidation may consume up to 4.60×10^8 mol day⁻¹ of TA in MAE. Nonetheless, these values should represent the upper limit of TA “sink” capacity given potentially faster oxidation rate in our experiment.

Due to the shallow nature of the estuary and overall high wind conditions (~ 7 m s⁻¹), TA consumption in MAE will be pronounced during periods of drought, when iron sulfides and other forms of reduced sulfur are exposed to oxic waters (Berner 1983; Howarth 1979; McKee et al. 2004). In sediment incubation and slurry experiments, carbonate dissolution partially diminished TA consumption signal. However, water column sampling results suggested that calcification occurred under natural conditions and in the presence of calcifying organisms (Fig. 4). As MAE is an important oyster habitat, and calcification was not captured in the lab incubation experiment, the TA consumption rate based on the lab incubations represent a rough estimate of natural TA consumption.

4.4 Caveats

In lab incubations, bioturbation and microbial activity under natural conditions were not replicated. However, bioturbation and sedimentary microbial communities may increase the rates of sulfide oxidation and the estimates of TA consumption due to sulfide oxidation reported here may be low (Jørgensen and Nelson 2004; Peterson et al. 1996; Schippers and Jørgensen 2002; van den Ende and Gemerden 1993). Additionally, in the natural environment (see Fig. 4), mixing of fresh and salt waters may have altered the ambient TA and [Ca²⁺] concentrations in between sampling times. For example, decline of high-TA river endmember waters to Copano Bay could also lead to the apparent TA consumption. This possible source of error warrants further investigation.

5 Conclusions

This study demonstrated that estuarine TA consumption in the semiarid MAE can be attributed to both calcification and oxidation of reduced sulfur species, which are more paramount during times of evaporation dominance (lagoonal state of estuary). A separate analysis (L. Dias, *unpublished data*) suggested that upstream human use of water resources is diminishing the quantity of freshwater inflow and TA entering this estuary over the long-term, and we expect these human demands on freshwater resources to increase as nearby population growth continues (Murdock et al. 2014). Additionally, climate change intensifies droughts, flooding, and storm events (AMS 2017), which may lead to extended periods of evaporation dominance and amplification of this TA consumption. Atmospheric CO₂ levels are projected to continue rising (Doney et al. 2020), with decades longer impacts on climate (AMS 2017). The effect of dilution or TA additions from terrestrial freshwater sources on estuarine TA also warrants further investigation.

Globally, subtropical estuaries extend poleward from the tropics (23.5° N or S) to approximately 30° latitudinal lines (Valle-Levinson et al. 2009). Reduced sulfur species including pyrite and iron sulfides are ubiquitous in marine sediments (Schippers and Jørgensen 2002) except in the carbonate-rich environment, and it is possible that similar TA

consumption may be occurring in other semi-enclosed subtropical estuaries throughout the world during periods of drought. This acid-driven TA consumption occurs in addition to acidification from CO₂ uptake, advection of acidified water from offshore, and TA consumption due to calcification. Therefore, TA loss may exacerbate acidification in the estuary during droughts when organisms are already stressed, which could have potentially negative impacts on estuarine organisms and ecosystems.

Supplementary Information The online version contains supplementary material available at <https://doi.org/10.1007/s10498-022-09410-z>.

Acknowledgements This work was supported by the 2020–2022 NOAA Ocean Acidification/Sea Grant Graduate Research Fellowship [award nos. NA14OAR4170102 and NA18OAR4170088] and NSF Chemical Oceanography Program (award no. OCE-1654232). We would like to thank the Mission-Aransas Estuary NERR for collection of precipitation data under an award from the Estuarine Reserves Division, Office of Ocean and Coastal Resource Management, National Oceanic and Atmospheric Administration. We would also like to thank J. David Felix, Alan Schiller, Dorina Murgulet, and Cory Staryk for their help with sample analyses.

Funding Funding was provided by NOAA Ocean Acidification Program and Sea Grant Program administered by Texas Sea Grant (award nos. NA14OAR4170102, NA18OAR4170088) and NSF Chemical Oceanography Program (award no. OCE-1654232).

Declarations

Conflict of interest The authors have no competing interests to declare that are relevant to the content of this article.

Open Access This article is licensed under a Creative Commons Attribution 4.0 International License, which permits use, sharing, adaptation, distribution and reproduction in any medium or format, as long as you give appropriate credit to the original author(s) and the source, provide a link to the Creative Commons licence, and indicate if changes were made. The images or other third party material in this article are included in the article's Creative Commons licence, unless indicated otherwise in a credit line to the material. If material is not included in the article's Creative Commons licence and your intended use is not permitted by statutory regulation or exceeds the permitted use, you will need to obtain permission directly from the copyright holder. To view a copy of this licence, visit <http://creativecommons.org/licenses/by/4.0/>.

References

- Abril G, Bouillon S, Darchambeau F, Teodoru R, Marwick TR, Tamooh F, Ochieng Omengo F, Geeraert N, Deirmendjian L, Polsenaerre P, Borges AV (2015) Technical note: large overestimation of *p*CO₂ calculated from pH and alkalinity in acidic, organic-rich freshwaters. *Biogeosciences* 12:67–78. <https://doi.org/10.5194/bg-12-67-2015>
- Aller RC, Rude PD (1988) Complete oxidation of solid phase sulfides by manganese and bacteria in anoxic marine sediments. *Geochim Cosmochim Acta* 52:751–765. [https://doi.org/10.1016/0016-7037\(88\)90335-3](https://doi.org/10.1016/0016-7037(88)90335-3)
- Amara V, Cabral HN, Bishop MJ (2012) Effects of estuarine acidification on predator-prey interactions. *Mar Ecol Prog Ser* 445:117–127. <https://doi.org/10.3354/meps09487>
- AMS (2017) State of the climate in 2016. In: Blunden J, Arndt DS, Diamond HJ, Dunn RJH, Gobron N, Hurst DF, Johnson GC, Mathis JT, Mekonnen A, Renwick JA, Richter-Menge JA, Sanchez-Lugo A, Scambos TA, Schreck CJI, Stammerjohn S, Willett KM (eds) *Bulletin of the American Meteorological Society*, vol 98, pp Si–S280. <https://doi.org/10.1175/2017BAMSStateoftheClimate.1>
- Berner A (1983) Sedimentary pyrite formation: an update. *Geochim Cosmochim Acta* 48:605–615. [https://doi.org/10.1016/0016-7037\(84\)90089-9](https://doi.org/10.1016/0016-7037(84)90089-9)
- Berner RA, Scott MR, Thomlinson C (1970) Carbonate alkalinity in the pore waters of anoxic marine sediments. *Limnol Oceanogr* 15:544–549. <https://doi.org/10.4319/lo.1970.15.4.0544>

- Bozkurt Z, Üzmez ÖÖ, Döğeroğlu T, Artun G, Gaga EO (2018) Atmospheric concentrations of SO₂, NO₂, ozone and VOCs in Düzce, Turkey using passive air samplers: sources, spatial and seasonal variations and health risk estimation. *Atmos Pollut Res* 9:1146–1156. <https://doi.org/10.1016/j.apr.2018.05.001>
- Bruesewitz DA, Gardner WS, Mooney RF, Pollard L, Buskey EJ (2013) Estuarine ecosystem function response to flood and drought in a shallow, semiarid estuary: nitrogen cycling and ecosystem metabolism. *Limnol Oceanogr* 58:2293–2309. <https://doi.org/10.4319/lo.2013.58.6.2293>
- Burdige DJ (1993) The biogeochemistry of manganese and iron reduction in marine sediments. *Earth Sci Rev* 35:249–284. [https://doi.org/10.1016/0012-8252\(93\)90040-E](https://doi.org/10.1016/0012-8252(93)90040-E)
- Burdige DJ (2007) *Geochemistry of Marine Sediments*. Princeton University Press, Princeton.
- Buzas-Stephens P, Buzas MA, Price JD, Courtney CH (2018) Benthic superheroes: living foraminifera from three bays in the Mission-Aransas National Estuarine Research Reserve, USA. *Estuaries Coast* 41:2368–2377. <https://doi.org/10.1007/s12237-018-0425-4>
- Cai WJ, Wang Y, Krest J, Moore WS (2003) The geochemistry of dissolved inorganic carbon in a surficial groundwater aquifer in North Inlet, South Carolina, and the carbon fluxes to the coastal ocean. *Geochim Cosmochim Acta* 67:631–637. [https://doi.org/10.1016/S0016-7037\(02\)01167-5](https://doi.org/10.1016/S0016-7037(02)01167-5)
- Canfield DE, Farquhar J (2009) Animal evolution, bioturbation, and the sulfate concentration of the oceans. *Proc Natl Acad Sci USA* 106:8123–8127. <https://doi.org/10.1073/pnas.0902037106>
- Canfield DE, Thamdrup B, Hansen JW (1993) The anaerobic degradation of organic matter in Danish coastal sediments: iron reduction, manganese reduction, and sulfate reduction. *Geochim Cosmochim Acta* 57:3867–3883. [https://doi.org/10.1016/0016-7037\(93\)90340-3](https://doi.org/10.1016/0016-7037(93)90340-3)
- Chong U, Swanson JJ, Boies AM (2015) Air quality evaluation of London Paddington train station. *Environ Res Lett*. <https://doi.org/10.1088/1748-9326/10/9/094012>
- Dickson AG, Afghan JD, Anderson GC (2003) Reference materials for oceanic CO₂ analysis: a method for the certification of total alkalinity. *Mar Chem* 80:185–197. [https://doi.org/10.1016/S0304-4203\(02\)00133-0](https://doi.org/10.1016/S0304-4203(02)00133-0)
- Dickson AG, Sabine CL, Christian JR (eds) (2007) *Guide to best practices for ocean CO₂ measurements*, PICES Special Publication 3. North Pacific Marine Science Organization, Sydney, Canada, 191 p. ISBN# 1-897176-07-4. https://www.nodc.noaa.gov/ocads/oceans/Handbook_2007/Guide_all_in_one.pdf
- Doney SC, Mahowald N, Lima I, Feely RA, Mackenzie FT, Lamarque J-F, Rasch PJ (2007) Impact of anthropogenic atmospheric nitrogen and sulfur deposition on ocean acidification and the inorganic carbon system. *Proc Natl Acad Sci USA* 104:14580–14585. <https://doi.org/10.1073/pnas.0702218104>
- Doney SC, Busch DS, Cooley SR, Kroeker KJ (2020) The impacts of ocean acidification on marine ecosystems and reliant human communities. *Annu Rev Environ Resour* 45:83–112. <https://doi.org/10.1146/annurev-environ-012320-083019>
- Dove MC, Sammut J (2007) Impacts of estuarine acidification on survival and growth of Sydney rock oysters *Saccostrea glomerata* (Gould 1850). *J Shellfish Res* 26:519–527. [https://doi.org/10.2983/0730-8000\(2007\)26\[519:IOEAOS\]2.CO;2](https://doi.org/10.2983/0730-8000(2007)26[519:IOEAOS]2.CO;2)
- Emerson S, Hedges J (2008) *Chemical Oceanography and the Marine Carbon Cycle*. Cambridge University Press, Cambridge. <https://doi.org/10.1017/CBO9780547932020>
- European Commission (2000) Directive 2000/53/EC of the European Parliament and of the Council 34–42. <https://www.legislation.gov.uk/eudr/2000/53/contents>
- Evans A, Madden K, Palmer SM (eds) (2012) *The Ecology and Sociology of the Mission-Aransas Estuary—an Estuarine and Watershed Profile*. University of Texas Marine Science Institute, Port Aransas, p 183
- Feely RA, Alin SR, Newton J, Sabine CL, Warner M, Devol A, Krembs C, Maloy C (2010) The combined effects of ocean acidification, mixing, and respiration on pH and carbonate saturation in an urbanized estuary. *Estuar Coast Shelf Sci* 88:442–449. <https://doi.org/10.1016/j.ecss.2010.05.004>
- Felix JD, Elliott EM (2014) Isotopic composition of passively collected nitrogen dioxide emissions: vehicle, soil and livestock source signatures. *Atmos Environ* 92:359–366. <https://doi.org/10.1016/j.atmosenv.2014.04.005>
- Garrels RM (1965) Silica: role in the buffering of natural waters. *Science* 48:69. <https://doi.org/10.1126/science.148.3666.69>
- Guo X, Cai WJ, Zhai W, Dai M, Wang Y, Chen B (2008) Seasonal variations in the inorganic carbon system in the Pearl River (Zhujiang) estuary. *Cont Shelf Res* 28:1424–1434. <https://doi.org/10.1016/j.csr.2007.07.011>
- Howarth RW (1979) Pyrite: its rapid formation in a salt marsh and its importance in ecosystem metabolism. *Science* 203:49–51. <https://doi.org/10.1126/science.203.4375.49>

- Hu X, Cai WJ (2011) An assessment of ocean margin anaerobic processes on oceanic alkalinity budget. *Glob Biogeochem Cycles* 25:1–11. <https://doi.org/10.1029/2010GB003859>
- Hu X, Pollack JB, McCutcheon MR, Montagna PA, Ouyang Z (2015) Long-term alkalinity decrease and acidification of estuaries in northwestern Gulf of Mexico. *Environ Sci Technol* 49:3401–3409. <https://doi.org/10.1021/es505945p>
- Hu X, Yao H, McCutcheon MR, Dias L, Staryk CJ, Wetz M, Montagna PA (2022) Aragonite saturation states in estuaries along a climate gradient in the northwestern Gulf of Mexico. *Front Env Sci* 10:951256. <https://doi.org/10.3389/fenvs.2022.951256>
- Hunter KA, Liss PS, Surapipith V, Dentener F, Duce R, Kanakidou M, Kubilay N, Mahowald N, Okin G, Sarin M, Uematsu M, Zhu T (2011) Impacts of anthropogenic SO_x, NO_x and NH₃ on acidification of coastal waters and shipping lanes. *Geophys Res Lett* 38:2–7. <https://doi.org/10.1029/2011GL047720>
- Isson TT, Planavsky NJ (2018) Reverse weathering as a long-term stabilizer of marine pH and planetary climate. *Nature*. <https://doi.org/10.1038/s41586-018-0408-4>
- Joesoef A, Kirchman DL, Sommerfield CK, Cai WC (2017) Seasonal variability of the inorganic carbon system in a large coastal plain estuary. *Biogeosciences* 14:4949–4963. <https://doi.org/10.5194/bg-14-4949-2017>
- Jørgensen BB (1977) The sulfur cycle of a coastal marine sediment (Limfjorden, Denmark). *Limnol Oceanogr* 22:814–832. <https://doi.org/10.4319/lo.1977.22.5.0814>
- Jørgensen BB, Nelson DC (2004) Sulfide oxidation in marine sediments: geochemistry meets microbiology. *Spec Pap Geol Soc Am* 379:63–81. <https://doi.org/10.1130/0-8137-2379-5.63>
- Jørgensen B, Bang M, Blackburn T (1990) Anaerobic mineralization in marine sediments from the Baltic Sea-North Sea transition. *Mar Ecol Prog Ser* 59:39–54. <https://doi.org/10.3354/meps059039>
- Kanamori S, Ikegami H (1980) Computer-processed potentiometric titration for the determination of calcium and magnesium in sea water. *J Oceanogr Soc Jpn* 36:177–184. <https://doi.org/10.1007/BF02070330>
- Krumins V, Gehlen M, Arndt S, Van Cappellen P, Regnier P (2013) Dissolved inorganic carbon and alkalinity fluxes from coastal marine sediments: model estimates for different shelf environments and sensitivity to global change. *Biogeosciences* 10:371–398. <https://doi.org/10.5194/bg-10-371-2013>
- Langdon C, Takahashi T, Sweeney C, Chipman D, Goddard J, Marubini F, Aceves H, Barnett H, Atkinson MJ (2000) Effect of calcium carbonate saturation state on the calcification rate of an experimental coral reef. *Glob Biogeochem Cycles* 14:639–654. <https://doi.org/10.1029/1999GB001195>
- Lee CS, Chang KH, Kim H (2018) Long-term (2005–2015) trend analysis of PM_{2.5} precursor gas NO₂ and SO₂ concentrations in Taiwan. *Environ Sci Pollut Res* 25:22136–22152. <https://doi.org/10.1007/s11356-018-2273-y>
- Liu Q, Charette MA, Breier CF, Henderson PB, McCorkle DC, Martin W, Dai M (2017) Carbonate system biogeochemistry in a subterranean estuary—Waquoit Bay, USA. *Geochim Cosmochim Acta* 203:422–439. <https://doi.org/10.1016/j.gca.2017.01.041>
- Luff R, Wallmann K (2003) Fluid flow, methane fluxes, carbonate precipitation and biogeochemical turnover in gas hydrate-bearing sediments at Hydrate Ridge, Cascadia Margin: Numerical modeling and mass balances. *Geochim Cosmochim Acta* 67:3403–3421. [https://doi.org/10.1016/S0016-7037\(03\)00127-3](https://doi.org/10.1016/S0016-7037(03)00127-3)
- Luther GW, Giblin A, Howarth RW, Ryans RA (1982) Pyrite and oxidized iron mineral phases formed from pyrite oxidation in salt marsh and estuarine sediments. *Geochim Cosmochim Acta* 46:2665–2669. [https://doi.org/10.1016/0016-7037\(82\)90385-4](https://doi.org/10.1016/0016-7037(82)90385-4)
- Mackenzie FT, Garrels RM (1966) Chemical mass balance between rivers and oceans. *Am J Sci* 264:507–525. <https://doi.org/10.2475/ajs.264.7.507>
- Marshall DJ, Santos JH, Leung KMY, Chak WH (2008) Correlations between gastropod shell dissolution and water chemical properties in a tropical estuary. *Mar Environ Res* 66:422–429. <https://doi.org/10.1016/j.marenvres.2008.07.003>
- McKee KL, Mendelsohn IA, Materne MD (2004) Acute salt marsh dieback in the Mississippi River deltaic plain: a drought-induced phenomenon? *Glob Ecol Biogeogr* 13:65–73. <https://doi.org/10.1111/j.1466-882X.2004.00075.x>
- Michalopoulos P, Aller RC (2004) Early diagenesis of biogenic silica in the Amazon delta: alteration, authigenic clay formation, and storage. *Geochim Cosmochim Acta* 68:1061–1085. <https://doi.org/10.1016/j.gca.2003.07.018>
- Middelburg JJ, Soetaert K, Hagens M (2020) Ocean alkalinity, buffering and biogeochemical processes. *Rev Geophys*. <https://doi.org/10.1029/2019RG000681>
- Millero FJ, Zhang JZ, Lee K, Campbell DM (1993) Titration alkalinity of seawater. *Mar Chem* 44:153–165. [https://doi.org/10.1016/0304-4203\(93\)90200-8](https://doi.org/10.1016/0304-4203(93)90200-8)

- Mooney RF, McClelland JW (2012) Watershed export events and ecosystem responses in the Mission-Aransas National Estuarine Research Reserve, South Texas. *Estuaries Coast* 35:1468–1485. <https://doi.org/10.1007/s12237-012-9537-4>
- Morse JW (1991) Oxidation kinetics of sedimentary pyrite in seawater. *Geochim Cosmochim Acta* 55:3665–3667. [https://doi.org/10.1016/0016-7037\(91\)90064-C](https://doi.org/10.1016/0016-7037(91)90064-C)
- Moses CO, Kirk Nordstrom D, Herman JS, Mills AL (1987) Aqueous pyrite oxidation by dissolved oxygen and by ferric iron. *Geochim Cosmochim Acta* 51:1561–1571. [https://doi.org/10.1016/0016-7037\(87\)90337-1](https://doi.org/10.1016/0016-7037(87)90337-1)
- Murdock SH, Cline ME, Zey M, Jeanty PW, Perez D (2014) Changing Texas: Implications of Addressing or Ignoring the Texas Challenge. Texas A&M University Press, College Station, p 251
- Murgulet D, Trevino M, Douglas A, Spalt N, Hu X, Murgulet V (2018) Temporal and spatial fluctuations of groundwater-derived alkalinity fluxes to a semiarid coastal embayment. *Sci Total Environ* 630:1343–1359. <https://doi.org/10.1016/j.scitotenv.2018.02.333>
- NIH (2022) PubChem. <https://pubchem.ncbi.nlm.nih.gov>. Accessed 18 Feb 2022
- Ogawa & Co., USA., Inc. (2006) NO, NO₂, NO_x and SO₂ Sampling Protocol Using the Ogawa Sampler. Ogawa & Co. USA., Inc., Pompano Beach, p 28
- Peterson GS, Ankley GT, Leonard EN (1996) Effect of bioturbation on metal-sulfide oxidation in surficial freshwater sediments. *Environ Toxicol Chem* 15:2147–2155. <https://doi.org/10.1002/etc.5620151210>
- Pollack JB, Yoskowitz D, Kim H, Montagna PA (2013) Role and value of nitrogen regulation provided by oysters (*Crassostrea virginica*) in the Mission-Aransas Estuary, Texas, USA. *PLoS ONE* 8:e65314. <https://doi.org/10.1371/journal.pone.0065314>
- Risgaard-Petersen N, Revil A, Meister P, Nielsen LP (2012) Sulfur, iron-, and calcium cycling associated with natural electric currents running through marine sediment. *Geochim Cosmochim Acta* 92:1–13. <https://doi.org/10.1016/j.gca.2012.05.036>
- Ryberg KR, Vecchia AV (2012) waterData—an R package for retrieval, analysis, and anomaly calculation of daily hydrologic time series data, version 1.0: U.S. Geological Survey Open-File Report 2012-1168. <https://doi.org/10.3133/ofr20121168>
- Schippers A, Jørgensen BB (2001) Oxidation of pyrite and iron sulfide by manganese dioxide in marine sediments. *Geochim Cosmochim Acta* 65:915–922. [https://doi.org/10.1016/S0016-7037\(00\)00589-5](https://doi.org/10.1016/S0016-7037(00)00589-5)
- Schippers A, Jørgensen BB (2002) Biogeochemistry of pyrite and iron sulfide oxidation in marine sediments. *Geochim Cosmochim Acta* 66:85–92. [https://doi.org/10.1016/S0016-7037\(01\)00745-1](https://doi.org/10.1016/S0016-7037(01)00745-1)
- Sillen LG (1961) The physical chemistry of seawater. AAAS Publication, Washington, pp 549–581
- Slaughter A, Ray S, Shattuck T (2020) International Maritime Organization (IMO) 2020 Strategies in a Non-compliant World. Deloitte Development LLC, pp 1–14
- Solis RS, Powell GL (1999) Hydrography, mixing characteristics, and residence times of Gulf of Mexico estuaries. In: Bianchi TS, Pennock JR, Twilley RR (eds) *Biogeochemistry of Gulf of Mexico estuaries*. Wiley, New York, pp 29–61
- TCEQ (2022) CAMS1070 monthly summary report. https://www.tceq.texas.gov/cgi-bin/compliance/monops/monthly_summary.pl?cams=1070. Accessed 3 Feb 2022
- TDWR (1982) Nueces and Mission-Aransas estuaries: an analysis of bay segment boundaries, physical characteristics, and nutrient processes. Austin, TX, USA, 73 p. https://www.twdb.texas.gov/publications/reports/limited_printing/doc/LP-083.pdf
- Thamdrup B, Finster K, Fossing H, Hansen JW, Jørgensen BB (1994) Thiosulfate and sulfite distributions in porewater of marine sediments related to manganese, iron, and sulfur geochemistry. *Geochim Cosmochim Acta* 58:67–73. [https://doi.org/10.1016/0016-7037\(94\)90446-4](https://doi.org/10.1016/0016-7037(94)90446-4)
- Tsyro S, Berge E (1997) The contribution of ship emission from the North Sea and the northeastern Atlantic Ocean to acidification in Europe. EMEP/MSC-W Note 4/97, 14 pp. Norwegian Meteorol Inst, Oslo
- TWDB (2021) Texas Water Development Board water data for Texas. <https://waterdatafortexas.org>. Accessed 10 Feb 2022
- USGS (2021) US Geological Survey water data for the nation. <https://waterdata.usgs.gov/nwis>. Accessed 26 Jan 2022
- Valle-Levinson A, Gutierrez de Velasco G, Trasviña A, Souza AJ, Durazo R, Mehta AJ (2009) Residual exchange flows in subtropical estuaries. *Estuaries Coast* 32:54–67. <https://doi.org/10.1007/s12237-008-9112-1>
- van den Ende FP, van Gemerden H (1993) Sulfide oxidation under oxygen limitation by a *Thiobacillus thioparus* isolated from a marine microbial mat. *FEMS Microbiol Ecol* 13:69–77. [https://doi.org/10.1016/0168-6496\(93\)90042-6](https://doi.org/10.1016/0168-6496(93)90042-6)
- Walden J, Pirjola L, Laurila T, Hatakka J, Pettersson H, Walden T, Jalkanen JP, Nordlund H, Truuts T, Meretoja M, Kahma KK (2021) Measurement report: characterization of uncertainties in fluxes and

- fuel sulfur content from ship emissions in the Baltic Sea. *Atmos Chem Phys* 21:18175–18194. <https://doi.org/10.5194/acp-21-18175-2021>
- Weatherall TF, Scheef LP, Buskey EJ (2018) Spatial and temporal settlement patterns of blue crab (*Callinectes sapidus* and *Callinectes similis*) megalopae in a drought-prone Texas estuary. *Estuar Coast Shelf Sci* 214:89–97. <https://doi.org/10.1016/j.ecss.2018.09.017>
- WHO (2010) WHO Guidelines for Indoor Air Quality: Selected Pollutants. Copenhagen, Denmark. <https://doi.org/10.1016/B978-0-12-384947-2.00550-X>
- Wolf-Gladrow DA, Zeebe RE, Klaas C, Körtzinger A, Dickson AG (2007) Total alkalinity: the explicit conservative expression and its application to biogeochemical processes. *Mar Chem* 106:287–300. <https://doi.org/10.1016/j.marchem.2007.01.006>
- Wong GTF (1979) Alkalinity and pH in the southern Chesapeake Bay and the James River estuary. *Limnol Oceanogr* 24:970–977. <https://doi.org/10.4319/lo.1979.24.5.0970>
- Yao H, Hu X (2017) Responses of carbonate system and CO₂ flux to extended drought and intense flooding in a semiarid subtropical estuary. *Limnol Oceanogr* 62:S112–S130. <https://doi.org/10.1002/lno.10646>
- Yin H, Aller JY, Furman BT, Aller RC, Zhu Q (2022) Cable bacteria activity and impacts in Fe and Mn depleted carbonate sediments. *Mar Chem* 246:104176. <https://doi.org/10.1016/j.marchem.2022.104176>

Publisher's Note Springer Nature remains neutral with regard to jurisdictional claims in published maps and institutional affiliations.